Uppsala Univeristy

Computational Physics - 1FA573

Final Project

Author: Fredriksson, Stina

Spring semester 2024

Contents

1 Project 1 & 2

1.1 Introduction

The main task of this project is to analyze particle scattering events, or more precisely the final scattering angle's dependency on the impact parameter. This is done both analytically by deriving the solution for square potential scattering and by approximating using numerical quadrature. An additional parameter which also will be studied is the effect of the relation between the initial kinetic energy and the potential, as well as the sign of the potential. The numerical approximations of the final scattering angle and the differential cross-section are also performed when using the Lennard Jones potential.

1.2 Background

To analyze the scattering event of a particle, it is necessary to define the set-up of the situation. This is demonstrated by figure 1 found below. A particle with the initial kinetic energy, E, approaches a potential. The parameter b in figure 1 is called the impact parameter and it is the perpendicular distance between the original straight trajectory of the particle and the center of potential. During a scattering event, the potential forces the projecting particle to change travelling direction by an angle which is referred to as the deflection angle. The final deflection, or scattering angle, is called Θ and it is dependent on different parameters of the set-up, such as the impact parameter b, initial kinetic energy E, and, of course, the potential.

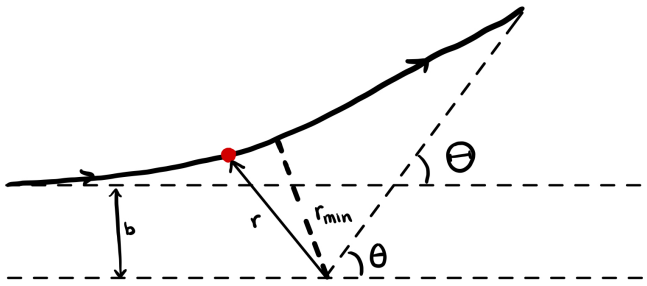

Figure 1: Set up of particle scattering event.

By utilizing conservation of angular momentum and the initial kinetic energy, it is possible to derive an expression for the deflection angle function.

$$L = mvb = mr^2 \frac{d\theta}{dt}$$

$$\frac{1}{2}m\left(\frac{dr}{dt}\right)^2 + \frac{L^2}{2mr^2} + V(r) = E$$

Rewriting these expressions and defining a bound r_{min} as the distance between the center potential and the particle's turning point, illustrated in figure 1, one can get

$$\Theta = \pi - 2b \int_{r_{min}}^{\infty} \frac{dr}{r^2} \left(1 - \frac{b^2}{r^2} - \frac{V(r)}{E}\right)^{-1/2}. \tag{1}$$

Once the particle has travelled far enough away from the potential, the deflection angle will become constant since the force on the particle from the potential will essentially become zero. At this point the distance between the particle and the potential is referred to as r_{max} and this is the upper bound of the expression above. It is possible to rewrite it by also using the following relation:

$$\text{When } V = 0 \text{ then } \Theta = 0 \text{ equation 1 becomes: } \pi = 2b \int_{b}^{\infty} \frac{dr}{r^2} \left(1 - \frac{b^2}{r^2}\right)^{-1/2} \implies$$

$$\Theta = 2b \left(\int_{b}^{r_{max}} \frac{dr}{r^2} \left(1 - \frac{b^2}{r^2}\right)^{-1/2} - \int_{r_{min}}^{r_{max}} \frac{dr}{r^2} \left(1 - \frac{b^2}{r^2} - \frac{V(r)}{E}\right)^{-1/2} \right) \tag{2}$$

Additional background about the potentials in the scattering events must be stated. The two potentials of interest are the square potential and the Lennard Jones potential. The square potential is defined as

$$V(r) = \begin{cases} U_0 & 0 \leq r \leq r_{max} \\ 0 & r > r_{max}. \end{cases} \tag{3}$$

Furthermore, is the Lennard Jones potential given by

$$V(r) = \begin{cases} 4V_0\left(\left(\frac{a}{r}\right)^{12} - \left(\frac{a}{r}\right)^{6}\right) & 0 \leq r \leq r_{max} \\ 0 & r > r_{max} \end{cases} \tag{4}$$

where $a = r_{max}/3$.

One interesting parameter of the expression for Θ which can be clarified further is r_{min}. As previously stated, it is defined as the closest distance between the center of potential and the particle during its trajectory. Due to this, it is determined by the r which yields in a zero value of the term in the second integral in equation 2. Hence, r_{min} is

$$1 - \frac{b^2}{r_{min}^2} - \frac{V(r_{min})}{E} = 0 \tag{5}$$

$$\text{For the square potential: } r_{min} = \frac{b}{\sqrt{1 - \frac{U_0}{E}}} \tag{6}$$

Finally, it is of essence to also introduce the differential cross section, $d\sigma/d\Omega$. This is a property of scattering events which can be measured experimentally. Its connection with the deflection angle of the scattering is expressed in equation 7 below. Since the aim of this project is to examine the interplay between the deflection angle, Θ, and the

impact parameter, b, then it is useful to acknowledge the connection to cross section by $d\Theta/db = (db/d\Theta)^{-1}$. [1]

$$\frac{d\sigma}{d\Omega} = \frac{b}{\sin\Theta}\left|\frac{db}{d\Theta}\right| \tag{7}$$

1.3 Analytical solution

The process of deriving the analytical solution to equation 2, namely $\Theta(b)$, demands performing a variable substitution of $p = b/r$:

$$p = \frac{b}{r}, \quad r = \frac{b}{p}, \quad dr = -\frac{b}{p^2}dp$$
$$p(r = r_{max}) = \frac{b}{r_{max}}, \quad p(r = b) = 1, \quad p(r = r_{min}) = \frac{b}{r_{min}}$$

Performing the substitution for the first integral of equation 2 yields in

$$\begin{aligned} 2b\int_b^{r_{max}} \frac{1}{r^2}\left(1 - \frac{b^2}{r^2}\right)^{-1/2} dr &= -2b\int_1^{b/r_{max}} \frac{1}{(\frac{b}{p})^2}\frac{1}{\sqrt{1 - \frac{b^2}{(\frac{b}{p})^2}}}\left(\frac{b}{p^2}\right) dp \\ &= 2\int_{b/r_{max}}^1 \frac{1}{\sqrt{1-p^2}}\,dp \\ &= 2\arcsin(p)\Big|_{b/r_{max}}^1 \\ &= \pi - 2\arcsin\left(\frac{b}{r_{max}}\right) \end{aligned} \tag{8}$$

When handling the second integral of equation 2 one must acknowledge the impact of the potential, $V(r)$. The analytical solution will be for the case of the square potential, i.e. $V(r) = U_0$ in the integral. Performing the substitution for the second integral yields in

$$\begin{aligned} 2b\int_{r_{min}}^{r_{max}} \frac{1}{r^2}\left(1 - \frac{b^2}{r^2} - \frac{U_0}{E}\right)^{-1/2} dr &= -2b\int_{b/r_{min}}^{b/r_{max}} \frac{1}{(\frac{b}{p})^2}\frac{1}{\sqrt{1 - \frac{b^2}{(\frac{b}{p})^2} - \frac{U_0}{E}}}\left(\frac{b}{p^2}\right) dp \\ &= 2\int_{b/r_{max}}^{b/r_{min}} \frac{1}{\sqrt{1 - p^2 - \frac{U_0}{E}}}\,dp \\ &= 2\arcsin\left(\frac{p}{\sqrt{1 - \frac{U_0}{E}}}\right)\Bigg|_{b/r_{max}}^{b/r_{min}} \\ &= 2\arcsin\left(\frac{b/r_{min}}{\sqrt{1 - \frac{U_0}{E}}}\right) - 2\arcsin\left(\frac{b/r_{max}}{\sqrt{1 - \frac{U_0}{E}}}\right). \end{aligned} \tag{9}$$

The first term can be rewritten using the definition of $r_{min} = b/\sqrt{1 - U_0/E}$ given in equation 6 gives

$$
\begin{aligned}
&= 2\arcsin\left(\frac{b\sqrt{1-\frac{U_0}{E}}/b}{\sqrt{1-\frac{U_0}{E}}}\right) - 2\arcsin\left(\frac{b/r_{max}}{\sqrt{1-\frac{U_0}{E}}}\right) \\
&= \pi - 2\arcsin\left(\frac{b}{r_{max}\sqrt{1-\frac{U_0}{E}}}\right)
\end{aligned} \tag{10}
$$

1.4 Analytical solution for $E < U_0$

If $E < U_0$ this means the particle will not have the sufficient amount of initial kinetic energy to enter the potential and therefor $r_{min} = r_{max}$. The second integral of the expression for Θ, equation 2, becomes zero due to this. Hence the analytical solution for $E < U_0$ is the first integral which was derived above to equation 8. If the impact parameter b is larger than r_{max} the particle will not become affected by the potential at all, thus $\Theta = 0$.

$$
\Theta(b, E < U_0) = \begin{cases} \pi - 2\arcsin\left(\frac{b}{r_{max}}\right), & 0 \leq b \leq r_{max} \\ 0, & b > r_{max} \end{cases} \tag{11}
$$

1.5 Analytical solution for $E > U_0$

Now for the case of $E > U_0$, the analytical solution is the difference between the two terms of equation 8 and 10. This leads to $\Theta = 2\arcsin\Big(b/(r_{max}\sqrt{1 - U_0/E})\Big) - 2\arcsin(b/r_{max})$ which first term is not defined for $b > r_{max}\sqrt{1 - U_0/E}$. It is therefore necessary to motivate what the analytical solution becomes for these values of b. At this situation the final scattering angle would be determined by not only the energy of the particle but also the incident angle which results in following the solution for this case:

$$
\Theta(b, E > U_0) = \begin{cases} 2\arcsin\left(\frac{b}{r_{max}\sqrt{1-\frac{U_0}{E}}}\right) - 2\arcsin\left(\frac{b}{r_{max}}\right), & 0 \leq b \leq r_{max}\sqrt{1 - U_0/E} \\ \pi - 2\arcsin\left(\frac{b}{r_{max}}\right), & r_{max}\sqrt{1 - U_0/E} < b \leq r_{max} \\ 0, & b > r_{max}. \end{cases} \tag{12}
$$

The analytical solutions of the two cases presented for particle scattering with square potential is plotted below in figure 2.

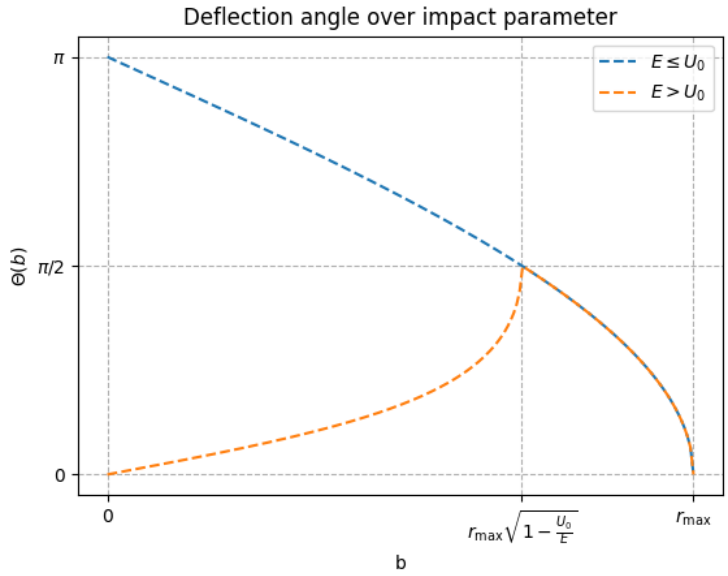

Figure 2: Plot of the analytical solution of the final scattering angle, Θ, for the case where $E < U_0$ and $E > U_0$ with regards to different impact parameters, b.

1.5.1 Analytical solution regarding the sign of U_0

If the sign of the potential is negative, the particle will be attracted instead of deflected. The system is conservative, with that means that the path integral inside the potential will be zero. Since the particle is entering the potential with a kinetic energy it will not close to an orbit but exit the potential. The second term of equation 10 will now not become undefined for $0 \leq b \leq r_{max}$ since in this case $r_{max} < r_{max}\sqrt{1 - U_0/E}$. This makes the analytical solution

$$\Theta(b, U_0 < 0) = \begin{cases} 2\arcsin\left(\frac{b}{r_{max}\sqrt{1-\frac{U_0}{E}}}\right) - 2\arcsin\left(\frac{b}{r_{max}}\right), & 0 \leq r \leq r_{max} \\ 0, & b > r_{max}. \end{cases} \tag{13}$$

1.6 Rewriting Θ for Numerical Approximation

To be able to use quadrature numerical approximation of the integrals of the scattering angle it is necessary to rewrite the integrals to avoid singularities. Lets remind what integral it is wished to make a numerical approximation of:

$$\Theta = 2b\left(\int_b^{r_{max}} \frac{dr}{r^2}\left(1-\frac{b^2}{r^2}\right)^{-1/2} - \int_{r_{min}}^{r_{max}} \frac{dr}{r^2}\left(1-\frac{b^2}{r^2}-\frac{V(r)}{E}\right)^{-1/2}\right)$$

The first integral is variable substituted by $p = \sqrt{r-b}$:

$$\begin{aligned} &p = \sqrt{r-b}, \quad r = p^2+b, \quad dr = 2p\,dp \\ &p(r=b) = 0, \quad p(r=r_{max}) = \sqrt{r_{max}-b}. \end{aligned}$$

Rewriting the first integral becomes now

$$2b\int_b^{r_{max}} \frac{1}{r^2}\left(1-\frac{b^2}{r^2}\right)^{-1/2} dr = 2b\int_0^{\sqrt{r_{max}-b}} \frac{1}{(p^2+b)^2}\frac{1}{\sqrt{1-\frac{b^2}{(p^2+b)^2}}} 2p\,dp \tag{14}$$

To numerically approximate the integral above through quadrature requires evaluation of $p = 0$ in the given expression. One can observe that this becomes undefined for the second factor. Thus, the limit of the expression as p approached zero must be determined.

$$\begin{aligned} \lim_{p\to 0} \frac{1}{(p^2+b)^2}\frac{1}{\sqrt{1-\frac{b^2}{(p^2+b)^2}}} 2p &= \lim_{p\to 0} \frac{2p}{(p^2+b)^2}\frac{(p^2+b)}{\sqrt{(p^2+b)^2-b^2}} \\ &= \lim_{p\to 0} \frac{2p}{(p^2+b)}\frac{1}{\sqrt{p^4+2p^2b}} \\ &= \frac{\sqrt{2}}{b\sqrt{b}} \\ &= \sqrt{2}\left(\frac{1}{b}\right)^{1.5} \end{aligned} \tag{15}$$

The second integral of equation 2 is variable substituted by $p = \sqrt{r-r_{min}}$:

$$\begin{aligned} &p = \sqrt{r-r_{min}}, \quad r = p^2+r_{min}, \quad dr = 2p\,dp \\ &p(r=r_{min}) = 0, \quad p(r=r_{max}) = \sqrt{r_{max}-r_{min}} \end{aligned}$$

Rewriting the second integral becomes now

$$2b\int_{r_{min}}^{r_{max}} \frac{1}{r^2}\left(1-\frac{b^2}{r^2}-\frac{V(r)}{E}\right)^{-1/2} dr = 2b\int_0^{\sqrt{r_{max}-r_{min}}} \frac{1}{(p^2+r_{min})^2}\frac{1}{\sqrt{1-\frac{b^2}{(p^2+r_{min})^2}-\frac{V(r)}{E}}}2p\,dp \tag{16}$$

Once again, the limit as p approaches zero must be determined:

$$\begin{aligned}
&\lim_{p\to 0}\frac{1}{(p^2+r_{min})^2}\frac{1}{\sqrt{1-\frac{b^2}{(p^2+r_{min})^2}-\frac{V(r)}{E}}}2p \\
&=\lim_{p\to 0}\frac{2p}{(p^2+r_{min})}\frac{1}{\sqrt{(p^2+r_{min})^2-b^2-\frac{V(r)}{E}(p^2+r_{min})^2}} \\
&=\lim_{p\to 0}\frac{2p}{(p^2+r_{min})}\frac{1}{\sqrt{(1-\frac{V(r)}{E})(p^2+r_{min})^2-b^2}} \\
&\overset{p^2\to 0}{\to}\lim_{p\to 0}\frac{2p}{r_{min}}\frac{1}{\sqrt{(1-\frac{V(r)}{E})(2p^2r_{min}+r_{min}^2)-b^2}}
\end{aligned} \tag{17}$$

To further evaluate the limit above the definition of $r_{min} = b/\sqrt{1-V(r)/E}$ (from equation 5) is used:

$$\begin{aligned}
&\lim_{p\to 0}\frac{2p(1-\frac{V(r)}{E})^{1/2}}{b}\frac{1}{\sqrt{2p^2b(1-\frac{V(r)}{E})^{1/2}+b^2-b^2}} \\
&=\lim_{p\to 0}\frac{2p(1-\frac{V(r)}{E})^{1/2}}{bp\sqrt{2b}(1-\frac{V(r)}{E})^{1/4}} \\
&=\frac{\sqrt{2}}{b\sqrt{b}}\left(1-\frac{V(r)}{E}\right)^{1/4}
\end{aligned} \tag{18}$$

The numerical integrals for approximating the final scattering angle Θ where $b \in [0, r_{max}]$ ultimately becomes

$$\begin{aligned}
\Theta(b) &= 2b\int_0^{\sqrt{r_{max}-b}} \frac{1}{(p^2+b)^2}\frac{1}{\sqrt{1-\frac{b^2}{(p^2+b)^2}}}2p\,dp \\
&-2b\int_0^{\sqrt{r_{max}-r_{min}}} \frac{1}{(p^2+r_{min})^2}\frac{1}{\sqrt{1-\frac{b^2}{(p^2+r_{min})^2}-\frac{V(r)}{E}}}2p\,dp
\end{aligned} \tag{19}$$

where when approximated through quadrature the limits must be used.

2 Method

To study the final scattering angle's dependence on the impact parameter, python scripts was developed with implementations of the analytical solution for the square potential using equation 11, 12 and 13 and the numerical integrals of equation 19. The integrals where approximated using Boole's rule of quadrature. For the case of the square potential the analytical solutions where used to analyze the error of the numerical approximation.

For the case of using Lennard Jones potential the analytical solution is not derived, but the numerical approximation is calculated using the integrals in equation 19 where $V(r)$ is equation 4. The approximation was evaluated for various $E : \{0.1V_0, 0.5V_0, V_0, 5V_0, 10V_0, 100V_0\}$. For this case the r_{min} is determined for each b and E through equation 5 by a numerical search of the root.

One additional important remark is what numerical value of Θ was appointed for $b = 0$. Since it was wished to examine $b \in [0, r_{max}]$ and the limits presented in equation 15 and 18 become undefined for $b = 0$ it was decided to cheat by letting the value be the analytical solution's value. So if $b = 0, E < U_0$ the value is $\Theta = \pi$ and if $b = 0, E > U_0$ the value is $\Theta = 0$.

To calculate the differential cross section it was done by approximating the differential of $d\Theta/db$ using the numerical Θ and apply equation 7. This was applied to the Lennard Jones potential. The approximation of the derivative was done by simply using $d\Theta/db \approx (\Theta(b + h) - \Theta(b - h))/2h$.

The Github repository of the project can be found below where the scripts `project1.py` and `project2.py` is for this study.

`https://github.com/stinafredriksson/Computational-Physics-Project/tree/main`.

3 Results

3.1 Deflection angle with the square potential

The analytical and numerical results for $E < U_0$:

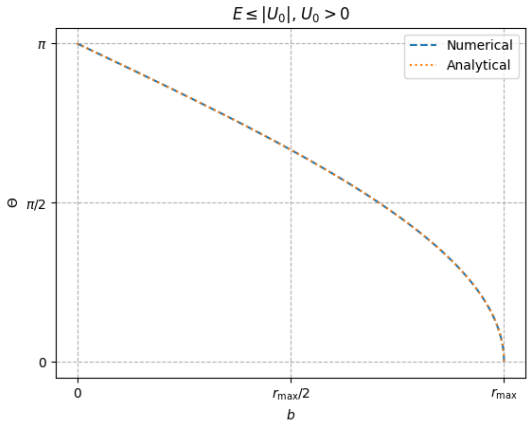

(a) Analytical and numerical Θ vs b for $E < U_0$.

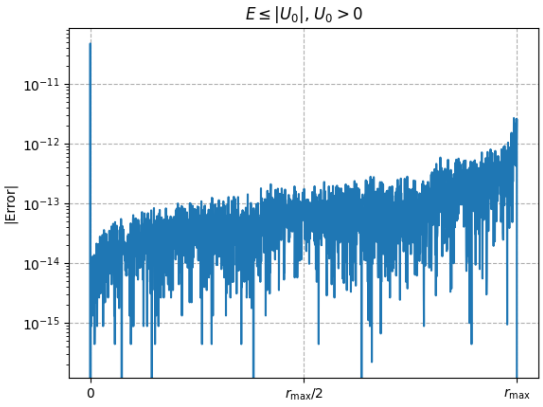

(b) The absolute error of numerical solution.

Figure 3: Analytical and numerical Θ for different impact parameter b and the error (absolute difference between analytical and numerical solution). The initial kinetic energy E of the particle is less than the potential U_0.

The analytical and numerical results for $E > U_0$:

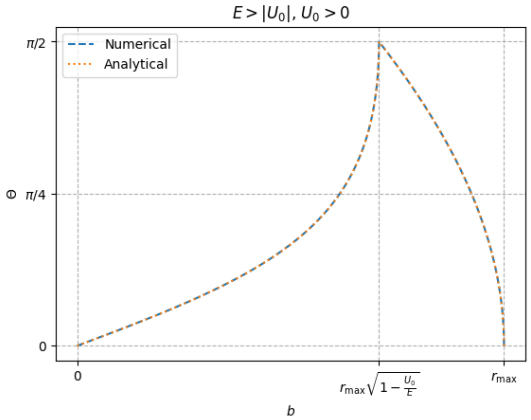

(a) Analytical and numerical Θ vs b for $E > U_0$.

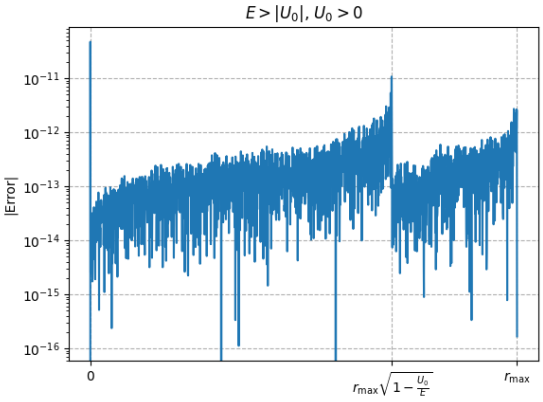

(b) The absolute error of numerical solution.

Figure 4: Analytical and numerical Θ for different impact parameter b and the error (absolute difference between analytical and numerical solution). The initial kinetic energy E of the particle is greater than the potential U_0.

The dependency on the sign of U_0:

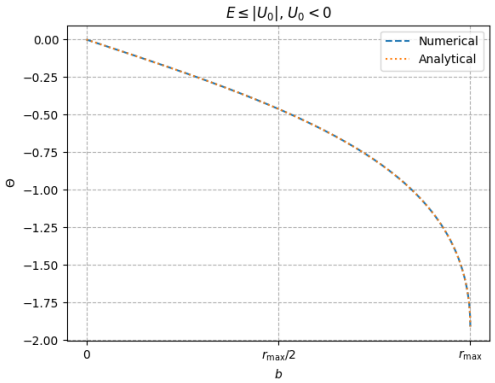

(a) Θ vs b for $E < |U_0|$, $U_0 < 0$.

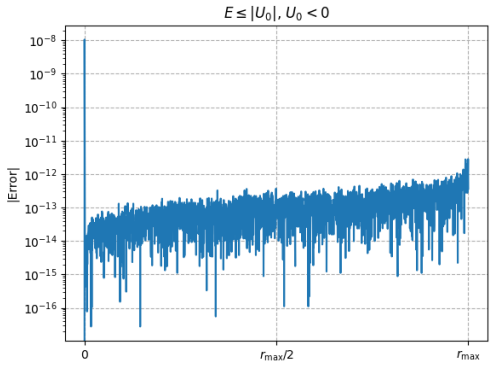

(b) The absolute error of numerical solution.

Figure 5: Analytical and numerical Θ for different impact parameter b and the error (absolute difference between analytical and numerical solution). The initial kinetic energy E of the particle is less than the absolute value of the potential U_0 and U_0 is negative.

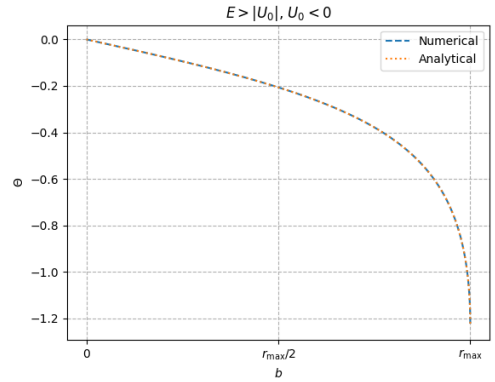

(a) Θ vs b for $E > |U_0|$, $U_0 < 0$.

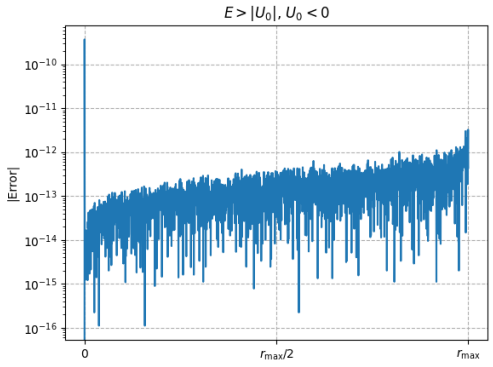

(b) The absolute error of numerical solution.

Figure 6: Analytical and numerical Θ for different impact parameter b and the error (absolute difference between analytical and numerical solution). The initial kinetic energy E of the particle is greater than the absolute value of the potential U_0 and U_0 is negative.

3.2 Deflection angle with the Lennard Jones potential

Numerical approximation of the final scattering angle Θ while varying b using the Lennard Jones potential and different values of the initial kinetic energy E:

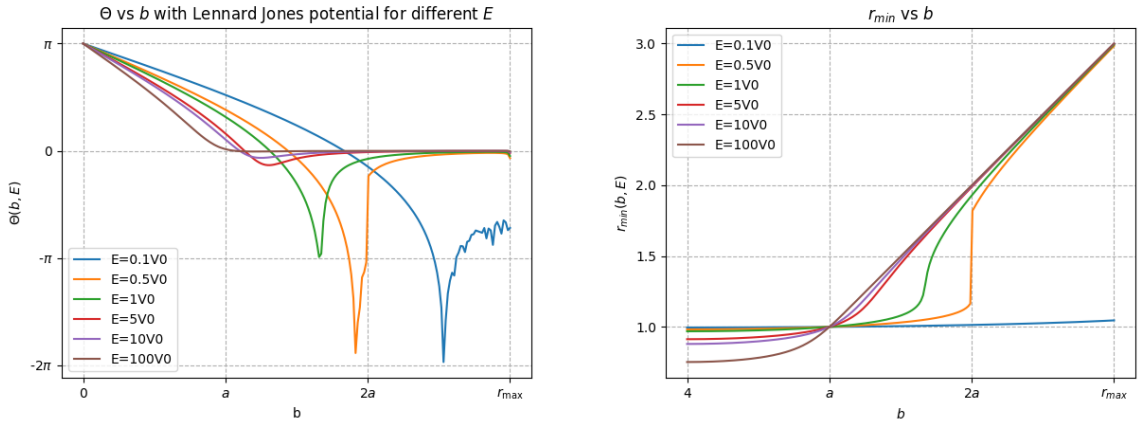

(a) Θ vs b for different E.

(b) r_{min} vs b for different E.

Figure 7: The numerical Θ using the Lennard Jones potential for different impact parameter b evaluated for different initial kinetic energy, E. The different r_{min} found for different b and E using numerical search to solve equation 5.

3.3 Differential cross-section for Lennard Jones potential

The different cross-sections' dependency on the impact parameter using numerical approximation of Θ with Lennard Jones potential evaluated for different initial kinetic energies:

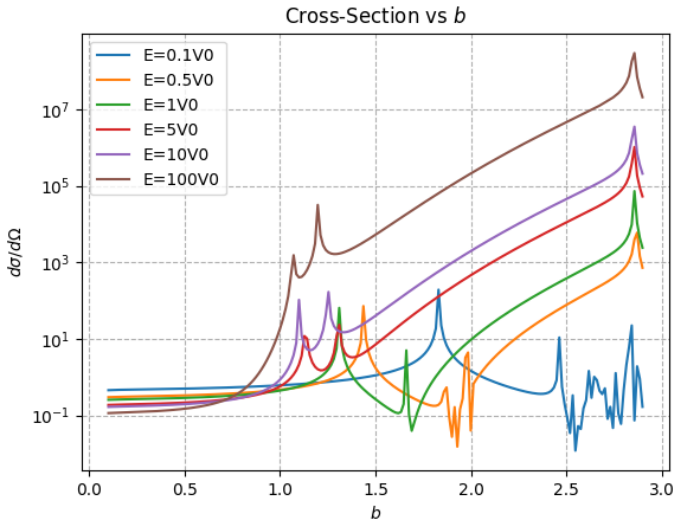

Figure 8: Differential cross-section vs b for different E.

4 Discussion

Examining the plots presented in figures 3 to 6 (scattering with square potenital) one can conclude that the numerical approximation follows the analytical solution very well. Also, the results can be intuitively motivated. For example of the case where the kinetic energy is less than the positive potential, figure 3, Θ goes from π to 0 as the impact parameter grows. This follows the reasoning that if a particle which does not have the energy to enter the potential collides perpendicular with the barrier (for $b = 0$), it will be affected by a force in the opposite of the traveling direction, thus change angle by 180°.

Also, for the case where U_0 is negative, the scattering angle becomes negative as the particle is now attracted by the potential, seen in figure 5 and 6.

Since the numerical approximation for the scattering event using a square potential turned out successful in comparison to the analytical solution, it is motivated to reason that the numerical method should work for the scattering event using the Lennard Jones potential. The potential differs in sign depending on r, hence when varying b it produces a turn in the graph for the scattering angle Θ, see in figure 7. This turn is most prominent for lower kinetic energy, which is believable since a particle with lower energy should be more and faster affected by the potential.

5 Project 3 & 4

6 Introduction

The main task of this project is to analyze the thermodynamic properties of a magnetic material by using the so called Ising model in two dimensions and Monte Carlo methods. The thermodynamic properties examined are magnetization, susceptibility and specific heat while varying the temperature and the size of the systems. This is done for ferro and antiferromagnetic material with and without an external magnetic field.

For the case of ferromagnetic material and a zero valued external field, the phase transition temperature is also obtained using the fourth order cumulants of the systems. Finally, the results and efficiency when using the Metropolis algorithm will be compared with when using the heat bath algorithm (for ferromagnetic material, no external magnetic field).

7 Background of the Ising model

The Ising model is for modelling magnetic behavior and is based on creating a big lattice of size $N_x \times N_y$ for the case of two dimensions. Each element in the lattice is referred to as a site, S_{ij} or more concise S_α, and the sites are valued either $+1$ or -1 corresponding to the "up´´ and "down´´ spin. This is illustrated in the figure below. The set-up of the model uses periodic boundary of the lattice.

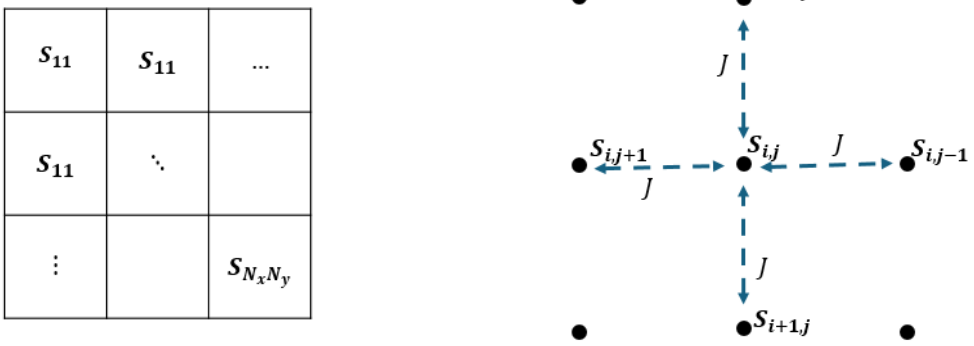

(a) Lattice with the sites $S_{i,j}$. ($+1 \sim$ spin up or -1 $\sim$ spin down).

(b) Spin interaction is by the nearest adjacent neighbours.

Figure 9: Set up of the Ising model in two dimensions.

If the strength of the spin interaction is J and the strength of the applied magnetic field is B, then the Hamiltonian of the Ising modelled system is defined as

$$\mathcal{H} = -J \sum_{\langle \alpha\beta \rangle} S_\alpha S_\beta - B \sum_\alpha S_\alpha. \tag{20}$$

The first sum denotes the sum over the system by taking the neighborhood sum of each site. The neighborhood sum $\langle\alpha\beta\rangle$ is defined as $\{S_{i,\pm1j}, S_{\pm1i,j}\}$. By analyzing the first term one can conclude that for $J > 0$ the energy of the system will be less if the neighborhood spins matches which is known as ferromagnetism.

The thermodynamic properties of the system are the following

$$\text{Magnetization: } M = \frac{\partial \log Z}{\partial B} = \sum_{\mathbf{S}} w(\mathbf{S}) \left(\sum_{\alpha} S_\alpha \right) \tag{21}$$

$$\text{Susceptibility: } \chi = \frac{\partial M}{\partial B} = \sum_{\mathbf{S}} w(\mathbf{S}) \left(\sum_{\alpha} S_\alpha \right)^2 - M^2 \tag{22}$$

$$\text{Energy: } E = \sum_{\mathbf{S}} w(\mathbf{S}) \mathcal{H}(\mathbf{S}) \tag{23}$$

$$\text{Specific heat constant: } C_B = \sum_{\mathbf{S}} w(\mathbf{S}) \mathcal{H}^2(\mathbf{S}) - E^2 \tag{24}$$

The weight function $w(\mathbf{S})$ is defined as

$$w(\mathbf{S}) = \frac{e^{-\mathcal{H}(\mathbf{S})}}{Z}, \text{ where the partition function is} Z(J, B) = \sum_{\mathbf{S}} e^{-\mathcal{H}(\mathbf{S})}. \tag{25}$$

Another property which should be introduced is the phase transition. The phase transition is when a material changes phase such as the transition from ferromagnetic to paramagnetic. The phase transition can be found as the intersection the different lattices' cumulants. The fourth order cumulant is

$$U_L = 1 - \frac{\langle M^4 \rangle_L}{3\langle M^2 \rangle_L^2} \tag{26}$$

where L is denoted as the size of the lattice. [1]

7.1 Metropolis algorithm

Monte Carlo methods works by utilizing a large sample of random points to combine and extract a mean which approximates the desired value. To perform this efficiently it is necessary to let the the random points generated follow a distribution, such as the weight function introduced in the previous section $w(\mathbf{S})$. For some cases the distribution is difficult or very computationally heavy, hence the method must be done in a different way. This is when the Metropolis algorithm comes in. [1]

For extracting the thermodynamic properties from the Ising model the Metropolis algorithm can be utilized. It follows the scheme [2]:

```
1. Choose an initial state.
2. Choose a site i.
3. Calculate the energy change dE, which occurs if the spin at i
```

```
   is flipped.
4. If dE<0, accept the move.
5. If dE>0, generate a random number r such that 0<r<1.
6. If r<exp(-dE/k_BT), flip the spin.
7. Go to the next site and got to step 3.
```

By using this it is possible to alter equations 21 to 24 which originally uses the exact weights $w(\mathbf{S})$ to the following when sampling measurements over N_S times

$$\text{Magnetization: } M \approx \frac{1}{N_S}\sum_{N_S}\left(\sum_{\alpha} S_\alpha\right) = \langle M \rangle \tag{27}$$

$$\begin{aligned}\text{Susceptibility: } \chi &\approx \frac{1}{N_s}\sum_{N_S}\left(\left(\sum_{\alpha} S_\alpha\right)^2\right) - \frac{1}{N_S}\sum_{N_S}\left(\sum_{\alpha} S_\alpha\right) \\ &= \frac{\langle M^2\rangle - \langle M\rangle^2}{k_B T}\end{aligned} \tag{28}$$

$$\begin{aligned}\text{Energy: } E &\approx \frac{1}{N_S}\sum_{N_S}\mathcal{H}(\mathbf{S}) = -\frac{1}{N_S}\sum_{N_S}\left(J\sum_{\langle\alpha\beta\rangle} S_\alpha S_\beta + B\sum_{\alpha} S_\alpha\right) \\ &= \frac{\langle E\rangle}{k_B T}\end{aligned} \tag{29}$$

$$\begin{aligned}\text{Specific heat constant: } C_B &\approx \frac{1}{N_S}\sum_{N_S}\mathcal{H}^2(\mathbf{S}) - \left(\frac{1}{N_S}\sum_{N_S}\mathcal{H}(\mathbf{S})\right)^2 \\ &= \frac{\langle E^2\rangle - \langle E\rangle^2}{k_B T^2}\end{aligned} \tag{30}$$

The constants are provided from Binder (1981).[3]

7.2 Heat bath algorithm

An alternative way of the Metropolis algorithm is the Heat bath algorithm. The Ising model can be simulated by the usage of this algorithm where the probability of a spin to be set up is referred to as p_i and without an external magnetic field it is

$$p_i = \frac{e^{2J\sum_j S_j/k_B T}}{1 + e^{2J\sum_j S_j}}/k_B T. \tag{31}$$

S_j's are the nearest neighbor spins.

7.3 Ferromagnetic and antiferromagnetic

Material can behave magnetically different depending on some properties. One categorization is ferromagnetic materials, where the spins of the system will align with each other. The system introduced above will behave ferromagnetically when the strength of the spin interaction J is greater than zero.

For the case $J < 0$ the system will behave antiferromagnetically. This will yield in the spins of the system will become anti-aligned and will cause the internal magnetization M to become zero. This is visualized in the figure below.

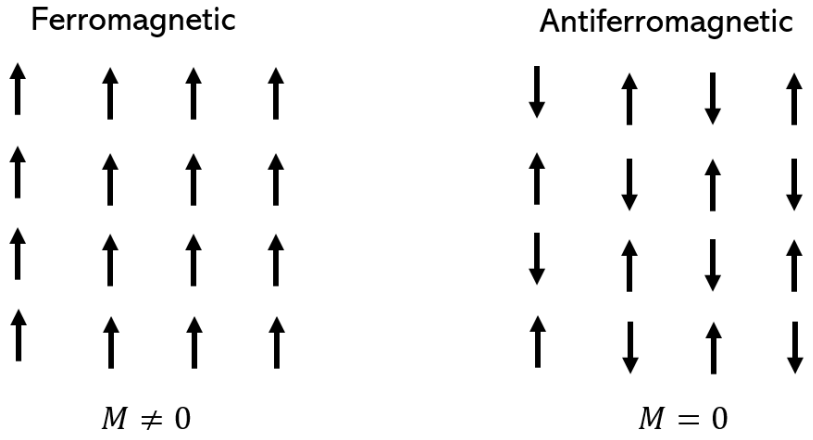

Figure 10: Ferromagnetic vs antiferromagnetic behavior.

These two different kinds of behaviors are only prominent below a certain transition temperature, T_c. Once over this point, the material will be dominantly affected by the thermal stochastic spin interaction rather than the magnetic. This relationship follows the expression, Curie-Weiss Law, presented in equation 32 where C is the Curie constant and B is the external field.

$$\chi = \frac{C}{T - T_c}, \qquad M = \chi B \tag{32}$$

Using the Ising model one can illustrate the ferromagnetic respectively antiferromagnetic behavior by showing the state of the system after applying the Metropolis algorithm. This is presented in figure 11 and 12 below.

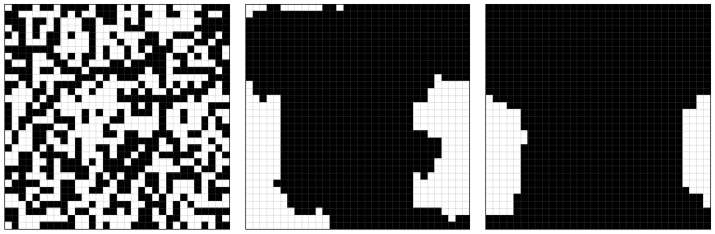

Figure 11: Metropolis Ising model for ferromagnetic material with a lattice of 32×32 and a random next site for step 1 (a), step 50000 (b) and step 100000 (c). The white squares have $S = 1$ and the black squares have $S = -1$.

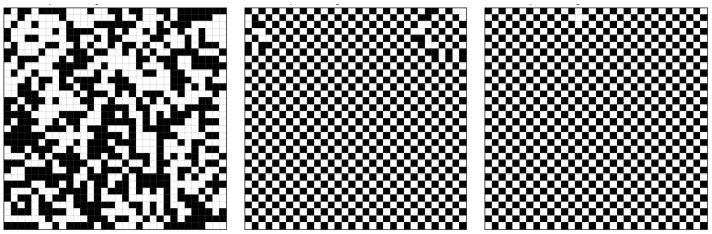

(a) (b) (c)

Figure 12: Metropolis Ising model for antiferromagnetic material with a lattice of 32×32 and a random next site for step 1 (a), step 50000 (b), step 100000 (c). The white squares have $S = 1$ and the black squares have $S = -1$.

7.4 Magnetic external field and the energy change

If no external magnetic field is applied the Hamiltonian expressed in equation 20 can be reduced to only one term as $B = 0$, view equation 33. The energy change when a spin at site α flips will be $\Delta\mathcal{H}$ in equation 34.

$$\mathcal{H} = -J \sum_{\langle \alpha\beta \rangle} S_\alpha S_\beta \tag{33}$$

$$\Delta\mathcal{H} = -J \sum_{\langle \alpha\beta \rangle} (-S_\alpha) S_\beta - \left(-J \sum_{\langle \alpha\beta \rangle} S_\alpha S_\beta \right) = 2JS_\alpha \sum_\beta S_\beta \tag{34}$$

Summing over β is summation over the two nearest adjacent neighbors of the element α.

If there is an external magnetic field applied to the system then $B \neq 0$ and the Hamiltonian will be as stated in equation 20. Calculating the energy change of a spin flip will now become

$$\begin{aligned} \Delta\mathcal{H} &= -J \sum_{\langle \alpha\beta \rangle} (-S_\alpha) S_\beta - \left(-J \sum_{\langle \alpha\beta \rangle} S_\alpha S_\beta \right) - B(-S_\alpha) - (-BS_\alpha) \\ &= 2BS_\alpha + 2JS_\alpha \sum_\beta S_\beta \end{aligned} \tag{35}$$

8 Method

The aim of this project was pursued by creating a code using the Ising model together with the Metropolis or Heat bath algorithm. The properties of equation 26 and 27 to 30 were sampled for ferro and antimagnetic material, with and without external magnetic field.

The study was performed for the different lattice sizes $\{4 \times 4, 8 \times 8, 16 \times 16, 32 \times 32\}$ and different temperatures (1-4K without B, 1-20K with B). For each temperature and lattice size, ten systems were simulated (using different random seeds). One very important aspect is that each system was first run 20 full lattice sweeps using the Metropolis (or Heat bath) algorithm to reach thermalization. After this, the properties can be sampled. They are measured 1000 times for each system with one sweep and $\mathcal{O}(N^2)$, Metropolis or Heat bath, steps between measurements to avoid correlation. The measurements are normalized by the number of lattice sites and the analytical critical temperature is calculated and is used for plotting.

For Metropolis algorithm, the calculation of the energy change `dE` is done using equation 35. To evaluate the Heat bath algorithm, the computation time for the simulation with heat bath and Metropolis steps was noted.

The code can be found in the scripts `project3_4.cpp` and `project3_4.py` in the Github repository. The modelling was first done using python, but was later on rewritten in C++ to make it faster, so the measurements could be averaged over a larger number of samples. The python file was in the end just used for plotting.

`https://github.com/stinafredriksson/Computational-Physics-Project/tree/main`

9 Results and Comments

9.1 Ferromagnetic material with no external field

For this run $J > 0$ and $B = 0$.

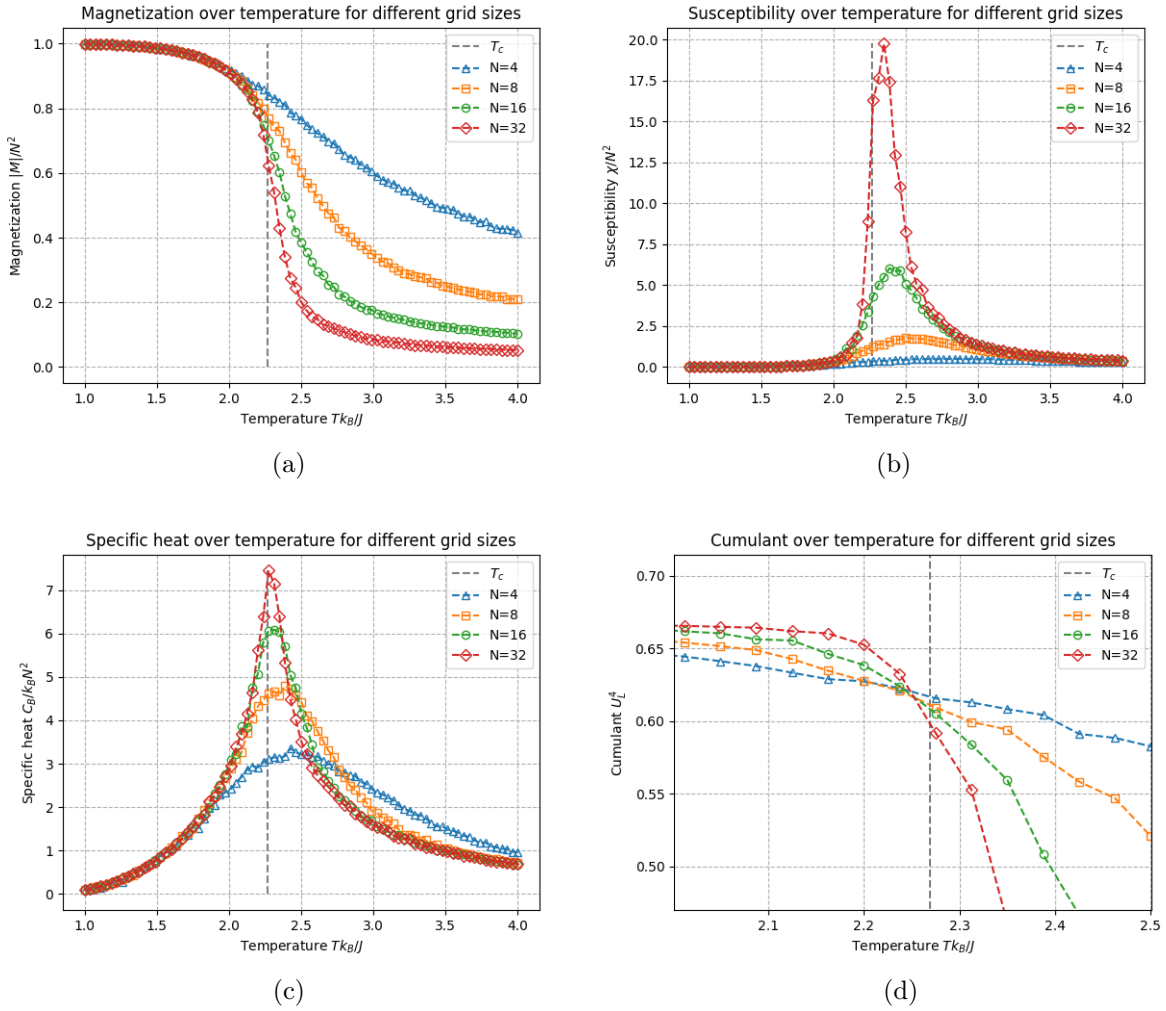

(a) (b)

(c) (d)

Figure 13: Thermodynamic properties and cumulant for ferromagnetic material with no external magnetic field applied using Metropolis algorithm. (a) Magnetization. (b) Susceptibility. (c) Specific heat capacity. (d) Fourth order cumulant.

The magnetization decreases as temperature arises above T_c which is motivated by theory, as here the thermal stochastic properties become dominant. Hence, the spins become unordered, which results in zero magnetization. Because of the ferromagnetic property, the spins are aligned at low temperature, which is why it starts at the value of one. Here it is also visible that the transition is more distinct for a bigger lattice, which is reasonable since for smaller lattices the boundary effects will be more prominent.

The susceptibility shows a peak around T_c and is highest for the bigger lattice. The specific heat capacity's trend acts similarly. This is explained by the fact that these properties are the difference of $\langle X^2 \rangle - \langle X \rangle^2$, which is also knows as the variance. By the transition temperature, the variance will be higher for larger lattices, since it has a higher number of possible different states as the system goes from ordered to unordered.

Regarding the fourth order cumulant, the phase transition is obtained by the intersection of the plots for the different lattices. The analytical calculation of T_c was approximately 2.269. In figure 13(d) the intersection can be extracted to be $2.24 \leq k_B T_c/J \leq 2.27$ and since the analytical value is in the range the approximation can be accepted.

9.2 Ferromagnetic material with no external field, using Heat bath algorithm

For this run $J > 0$ and $B = 0$.

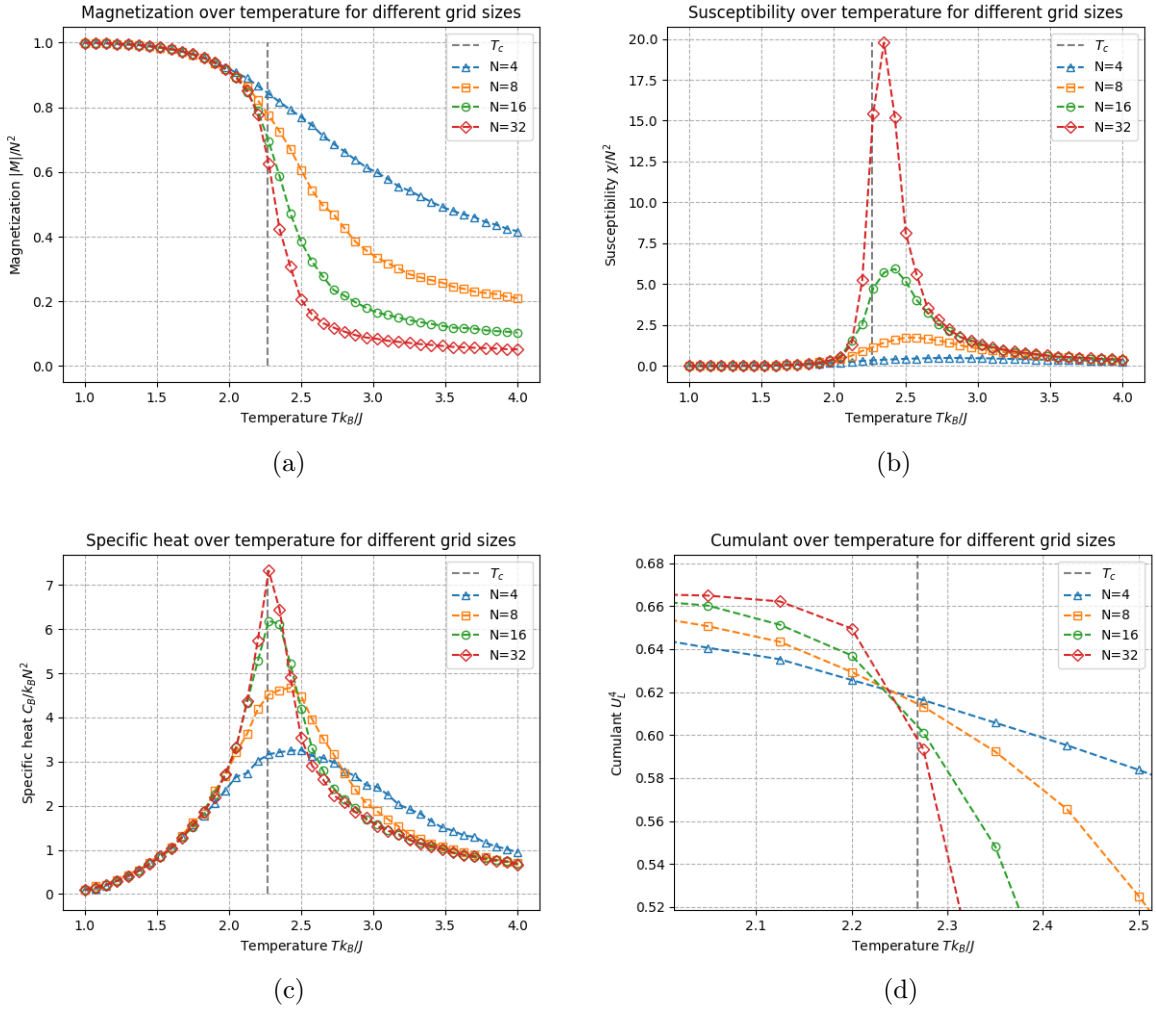

Figure 14: Thermodynamic properties and cumulant for ferromagnetic material with no external magnetic field applied using Heat bath algorithm. (a) Magnetization. (b) Susceptibility. (c) Specific heat capacity. (d) Fourth order cumulant.

The main aim of examining the model using the Heat bath algorithm is to evaluate if it produced the same results as Metropolis and the efficiency. Comparing figure 13 and 14 it can be concluded that they portray the same results. The time for the Heat bath run took 10 minutes and 23 seconds, whereas for the Metropolis algorithm it took 8 minutes and 46 seconds. This shows a higher efficiency for the Metropolis algorithm.

9.3 Antiferromagnetic material with no external field

For this run $J < 0$ and $B = 0$.

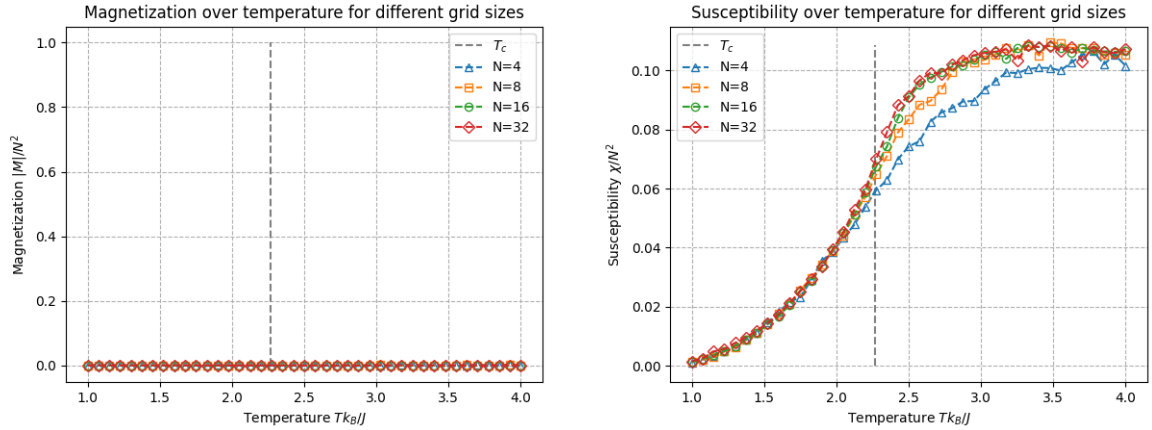

(a)

(b)

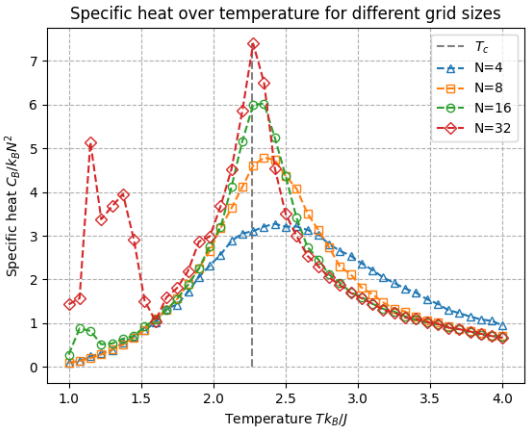

(c)

Figure 15: Thermodynamic properties for antiferromagnetic material with no external magnetic field applied using Metropolis algorithm. (a) Magnetization. (b) Susceptibility. (c) Specific heat capacity.

Firstly, the magnetization stays stable around zero while varying the temperature for all lattice sizes. This is understandable since the spins are anti aligned for antiferromagnetic material, which results in zero magnetization. When the model transitions to higher temperature the states will be unordered due to thermal energy which also results in zero magnetization. The susceptibility presents an increase and stabilizes at around 0.10. The specific heat behaves as for the ferromagnetic case.

9.4 Ferromagnetic and antiferromagnetic material with an external field

For this run $J > 0$ and $B = k_B$.

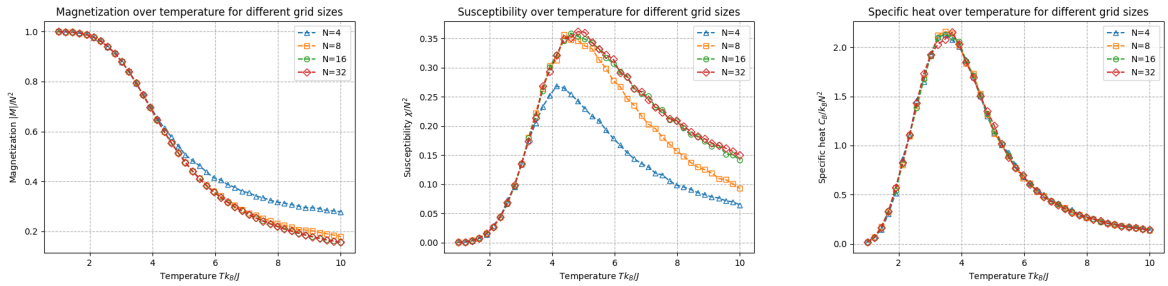

(a) (b) (c)

Figure 16: Thermodynamic properties for ferromagnetic material with an external magnetic field applied using Metropolis algorithm. (a) Magnetization. (b) Susceptibility. (c) Specific heat capacity.

For this run $J < 0$ and $B = k_B$.

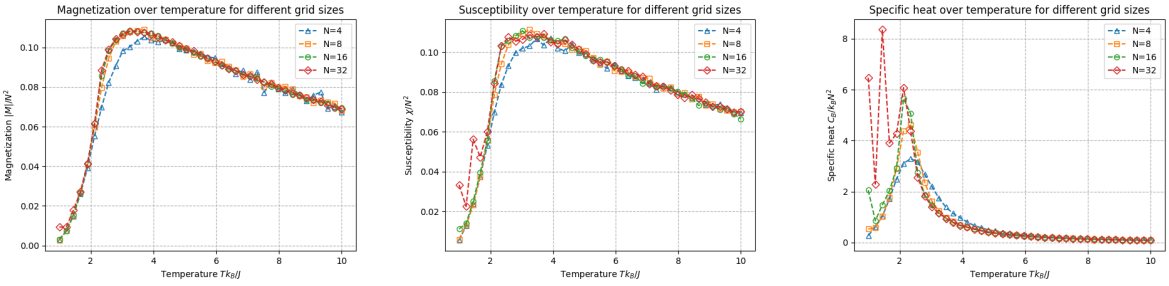

(a) (b) (c)

Figure 17: Thermodynamic properties for antiferromagnetic material with an external magnetic field applied using Metropolis algorithm. (a) Magnetization. (b) Susceptibility. (c) Specific heat capacity.

For the ferromagnetic case in figure 16 one can compare it to the figure without the external field, figure 13. For all properties, the transition is widened. With an external field, the temperature is ranged between 1 and 20 to be able to view the change. The magnetization behaves similarly, but for both the susceptibility and specific heat capacity, the run with an external field produces lower values. The plots are not as sharp, and it does not seem to vary as much regarding the lattice size.

For the antiferromagnetic material, it is now possible to see that the magnetization is no longer constantly zero, as in figure 17(a). This is in line with the fact that the external field contributes to the magnetization. The susceptibility in figure 17 is now more similar to the ferromagnetic case.

References

1. Koonin SE and Meredith DC. Computational Physics: Fortran Version. Westview Press, 1998
2. Sanyal B. Lecture 7 notes in Computational Physics. 2023 Feb
3. Binder K. Finite Size Scaling Analysis of Ising Model Block Distribution Functions. *Finite-Size Scaling*. Ed. by CARDY JL. Vol. 2. Current Physics–Sources and Comments. Elsevier, 1988 :79–100. DOI: https://doi.org/10.1016/B978-0-444-87109-1.50012-1